Distorted iron films on GaAs(001)-(4×6)

R. A. Gordon, E. D. Crozier,* D.-T. Jiang, T. L. Monchesky, and B. Heinrich
Department of Physics, Simon Fraser University, Burnaby, British Columbia, Canada V5A 1S6
(Received 27 December 1999)

Polarized *K*-edge x-ray absorption fine structure spectroscopy (XAFS) studies were performed both *in* and *ex situ* on iron films deposited on GaAs substrates. Samples with 5 and 10 ML (monolayers) of iron deposited on sulfur-passivated and (4×6)-reconstructed GaAs(001) surfaces, respectively, were studied *ex situ* (capped with 20 ML of gold) and compared with 9.3 ML on GaAs(001)-(4×6) measured *in situ*. Analysis of XAFS spectra for both samples on (4×6)-GaAs reveals a tetragonal distortion of the iron film relative to bulk body-centered-cubic iron. The distortion involves an in-plane contraction and an expansion perpendicular to the GaAs surface to give a c/a ratio of 1.03(1), with a comparable to half the bulk lattice constant of GaAs. The sample on sulfur-passivated GaAs did not exhibit this distortion.

I. INTRODUCTION

Significant efforts have been made to understand the physical and magnetic behavior of iron films on gallium arsenide.[1–6] The appeal of this system is the very small lattice mismatch between body-centered-cubic (bcc) iron ($a=2.866$ Å) and GaAs ($a/2=2.827$ Å). Having only a 1.4% mismatch should facilitate the growth of bcc-like Fe films on the GaAs substrate, making this system ideal for testing new thin-film structures for magnetoelectronic applications.[7,8]

Complications to studies of this system, in the form of magnetically-dead layers arise from reaction of the iron with the GaAs to form a solid solution, $Fe_3Ga_{2-x}As_x$[9,10] at the interface and, depending on preparation conditions, to several tens of monolayers in thickness.[9] Two approaches exist to avoid forming this ternary phase at the interface: sulphur passivation[11,12] and Ga enrichment of the GaAs surface by using the (4×6) reconstruction.[13,14] Both are aimed at reducing the availability of As for reaction with the Fe and at producing bcc-structured Fe films.

Recently, Monchesky *et al.*[15] described a method, modified from Zölfl *et al.*,[13] for preparing high-quality Fe films on GaAs(001)-(4×6) for iron thicknesses greater than 4 ML (monolayers). Using polarization-dependent x-ray absorption fine-structure spectroscopy (XAFS),[16–21] we can examine the structure of the iron film both in plane, and extract information complimentary to the electron diffraction techniques, reflection high-energy electron diffraction (RHEED) or low-energy electron diffraction and perpendicular to the surface, a direction in which interpreting results from the electron techniques is more involved. We have examined *ex situ* a 10 ML iron film on GasAs(001)-(4×6) capped with 20 ML of gold [20Au/10Fe/GaAs(001)-(4×6)] using polarized XAFS and compared it to *in situ* results on a 9.3 ML sample [9.3Fe/GaAs(001)-(4×6)] that are preliminary to an extended *in situ* study.[22] Measurements for further comparison have also been made on a 5 ML gold-capped iron film on a sulfur-passivated GaAs(001) substrate (20Au/5Fe/GaAs-S-pass).

II. EXPERIMENT

Samples on (4×6)-GaAs were prepared by molecular-beam epitaxy on epiready GaAs (American Xtal Technology) as described in Ref. 15. Briefly, the wafer sections were sputtered using an Ar^+ beam (500 eV) for several hours at room temperature (with azimuthal rotation of the crystal) and subsequently annealed under ultrahigh vacuum (UHV) conditions until the (4×6) reconstruction was observed by RHEED. Deposition of the iron was performed at room temperature at a rate of approximately 1 ML/min and monitored by RHEED with the number of oscillations of the specular (anti-Bragg) spot intensity giving the film thickness. The sulfur-passivated sample was prepared by treatment with aqueous ammonium sulfide, rinsed and dried prior to introduction to the vacuum system as described in Ref. 12. Samples for *ex situ* measurements, prepared by the Heinrich group at Simon Fraser University, also had 20 ML of gold epitaxially grown on top of the iron for protection from the atmosphere and were stored under anhydrous conditions until measurement.

Iron *K*-edge XAFS measurements were performed at the PNC-CAT undulator beamline,[23] Sector 20, at the Advanced Photon Source, Argonne National Laboratory. Linearly polarized x-rays from a Si-(111) double crystal monochromator (60% tune at 7500 eV) were incident on the films at 0.25° (~5/8 the critical angle for total reflection) for *in situ* or near glancing angle ($\lesssim2°$) for *ex situ* measurements. Fluorescent x rays were monitored by an Ar-filled (1 atm), five-electrode (Ni-mesh) ionization chamber[21] located at 90° to the x-ray beam in the direction of the polarization vector for *ex situ* measurements and by a smaller cylindrical detector of similar (but UHV compatible) design[24] at 60° to the beam and 30° to the polarization for the *in situ* fluorescence detection. Transmission measurements on a 7.5 μm thick iron foil were also made for reference using He-filled, two-parallel-plate-electrode ionization chambers.

The electric-field vector of the x-rays was within 2° of the (001) direction for out-of-plane measurements on the three samples. In-plane measurements were done roughly along the (110) and (010) directions for *ex situ* and *in situ* samples, respectively. Small azimuthal adjustments (within 2°) were made to shift the positions of Bragg peaks contaminating the XAFS to permit better peak removal before averaging the spectra.

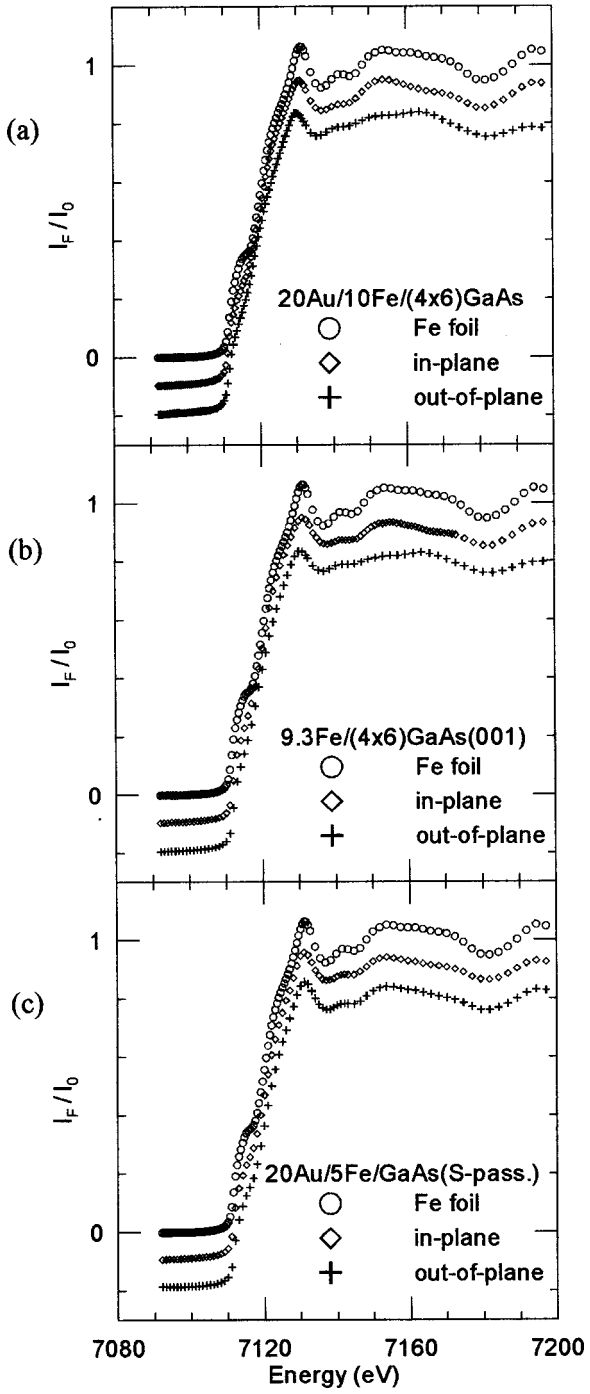

FIG. 1. Polarization dependent Fe *K*-edge XANES of (a) 20Au/10Fe/GaAs(001)(4×6) (*ex situ*), (b) 9.3Fe/GaAs(001)(4×6) (*in situ*), and (c) 20Au/5Fe/GaAs(001) (S passivated, *ex situ*) samples compared with iron foil. The electric-field vector of the x rays was either parallel (in-plane) or perpendicular (out-of-plane) to the substrate. Data has been offset vertically in 0.1 increments for clarity.

III. RESULTS

Figure 1 shows the x-ray absorption near-edge structure (XANES) for the three samples (20Au/10Fe/GaAs(001)-(4×6), 9.3Fe/GaAs(001)-(4×6), and 20Au/5Fe/GaAs(001)-S-passivated) compared to iron foil with the x-ray electric-field vector parallel (in-plane) or perpendicular (out-of-plane) to the GaAs substrates. The monochromator

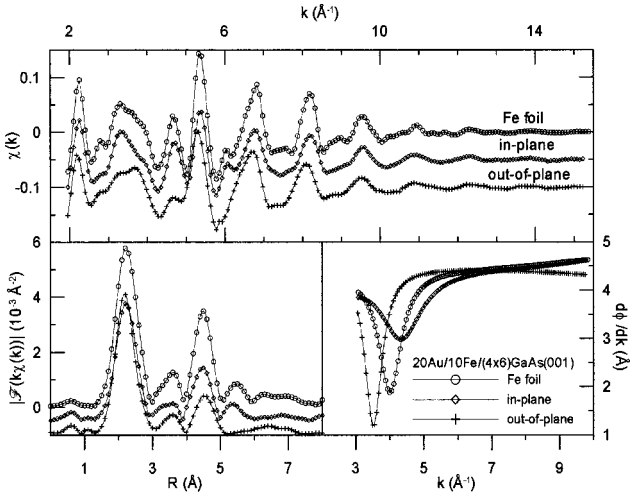

FIG. 2. Counterclockwise from top: XAFS $\chi(k)$, magnitude of the Fourier transform, $\mathcal{F}[k\chi(k)]$, and the derivative of the phase of the inverse transform of the first peak for 20Au/10Fe/GaAs(001)(4×6).

was calibrated such that the onset for the edge (first maximum in the derivative) in the foil (E_0) was defined to be 7112 eV. The edge energies for the thin-film samples are consistent with the foil's edge energy, indicating no change in valence for the iron in the thin films. Above the edge, the XANES for the 5 ML of Fe on sulfur-passivated GaAs resembles quite strongly that for the iron foil. The XANES for the samples on (4×6)-GaAs, while exhibiting features similar to those for the foil, do show some differences that are more pronounced for the out-of-plane measurements than those for the measurements made with the x-ray electric-field vector in the plane of the film. This all suggests that the structure of the iron films is similar to that for bcc iron, with some distortion for the samples on (4×6)-GaAs.

The EXAFS interference functions $\chi(k)$, shown in Figs. 2 through 4 were extracted from the $\mu(E)$ data of individual scans using a polynomial background subtraction and normalization to edge jump.[25] The $\chi(k)$ shown are averages of five scans for out-of-plane, three for in-plane measurements,

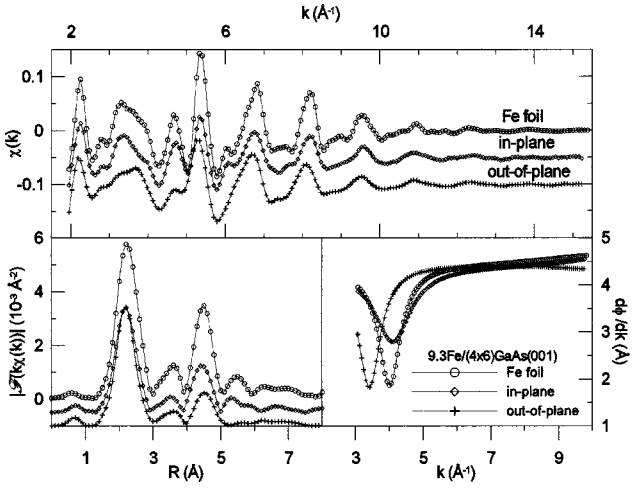

FIG. 3. Counterclockwise from top: XAFS $\chi(k)$, magnitude of the Fourier transform, $\mathcal{F}[k\chi(k)]$, and the derivative of the phase of the inverse transform of the first peak for 9.3Fe/GaAs(001)(4×6).

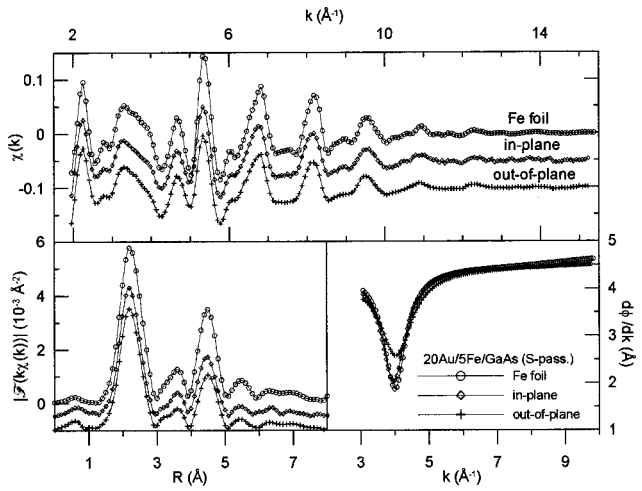

FIG. 4. Counterclockwise from top. XAFS $\chi(k)$, magnitude of the Fourier transform, $\mathcal{F}[k\chi(k)]$, and the derivative of the phase of the inverse transform of the first peak for 20Au/5Fe/GaAs(001) S passivated.

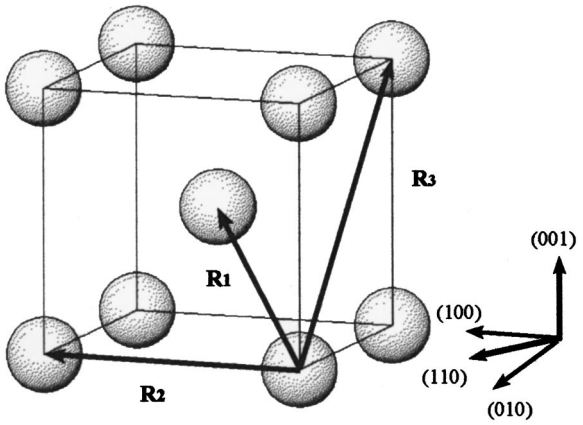

FIG. 5. bcc iron unit cell showing representative atoms for the first three backscattering paths: R_1—nearest neighbor, R_2—lattice parameter, and R_3—face-diagonal distances.

and two for the foil. Fourier transforms in these figures were taken with k^1 weighting and a 10% Gaussian window over the k-space range using the nearest zero crossings to 3 and 15 Å^{-1}. Inverse transforms of the first peak were taken typically over the range 1.65 to 2.85 Å to examine interference effects (beating) between the nearest and second-nearest neighbors. The phases of the inverse transform have been differentiated with respect to $k\{k=\hbar^{-1}\sqrt{[2m_e(E-E_0)]}\}$ and plotted with the EXAFS spectra and Fourier transforms for beating analysis.[26,27]

The first- and second-nearest neighbors in bcc iron (Fig. 5), at $R_1=2.4824$ Å and $R_2=2.8664$ Å (note: $R_2=a$, the lattice parameter), cause the beating observed from the first peak in the Fourier transform of $k\chi(k)$. The k values corresponding to the minima in the derivatives of the phase shown in Figs. 2–4 are related approximately to the separations between R_1 and R_2 for the foil and samples by the relation[26,27]

$$k_{\min}\times(R_2-R_1)=\text{const} \tag{1}$$

provided the two neighbors are the same element. Ideally, the constant would be $\pi/2$, however, the transform range, disorder, alloying, the presence of a substrate, and a passivation layer or capping layer may all influence the difference in distances for our samples.

Taking the iron foil as a reference to give the *constant* term, and $k_{\min}$ from the derivatives of the phase, $d\phi/dk$, shown in Figs. 2–4, we obtain the values listed in Table I for the differences in distance. Also listed in Table I are estimates of the lattice parameters using the bulk-iron crystallographic value of R_1. Consistent with the XANES, the 5 ML sample on S-passivated GaAs shows little difference (possibly a slight in-plane expansion and out-of-plane contraction) from bcc iron while the samples on (4×6)-GaAs exhibit a small in-plane contraction and larger out-of-plane expansion. The beating analysis provides an initial model for further analysis: a body-centered-tetragonal (bct) distortion from body-centered-cubic iron with space group I4/mmm, $a=2.84$ Å and $c=2.92$ Å for the samples on (4×6)-GaAs, and no distortion from bcc for the 5 ML sample on S-passivated GaAs.

Before continuing the analysis, and even though the $\chi(k)$ bears a strong resemblance to that for bulk iron, it was necessary to consider the possibility of the formation of the ''$Fe_3Ga_{2-x}As_x$'' compound. Using the computer program, FEFF7,[28] to generate electron-scattering amplitudes and phase shifts, EXAFS simulations were made of both bcc iron and a representative composition of the ternary solid solution $Fe_{3.22}Ga_{1.83}As_{0.32}$.[29] To prepare the simulations, a Debye temperature of 470 K corresponding to bulk iron, was used with the temperature set at 300 K. The final $\chi(k)$ for the ternary composition was a weighted sum of the contributions

TABLE I. Beating analysis results for samples 20Au/10Fe/(4×6)-GaAs, 9.3Fe/(4×6)-GaAs, and 20 Au/5Fe/GaAs (S passivated) referenced to iron foil. The known crystallographic distances were used for iron foil R values. In all cases, R_1 was taken to be that for iron foil (2.4824 Å). Random errors quoted come from locating $k_{\min}$ and do not include other sources.

Parameter	Fe foil	20Au/10Fe	9.3Fe	20Au/5Fe (S)
$k_{\min}$ (in plane, Å^{-1})	4.003(5)	4.332(5)	4.132(8)	3.961(8)
R_2-R_1 (Å)	0.3840	0.355(1)	0.372(1)	0.388(1)
$R_2=a$ (Å)	2.8664	2.837(1)	2.854(1)	2.870(1)
$k_{\min}$ (out-of-plane)	4.003(5)	3.519(6)	3.409(7)	4.036(9)
R_2-R_1 (Å)	0.3840	0.437(2)	0.451(1)	0.381(1)
$R_2=c$ (Å)	2.8664	2.919(2)	2.933(1)	2.863(1)
c/a	1.000	1.029(1)	1.028(1)	0.9976(7)

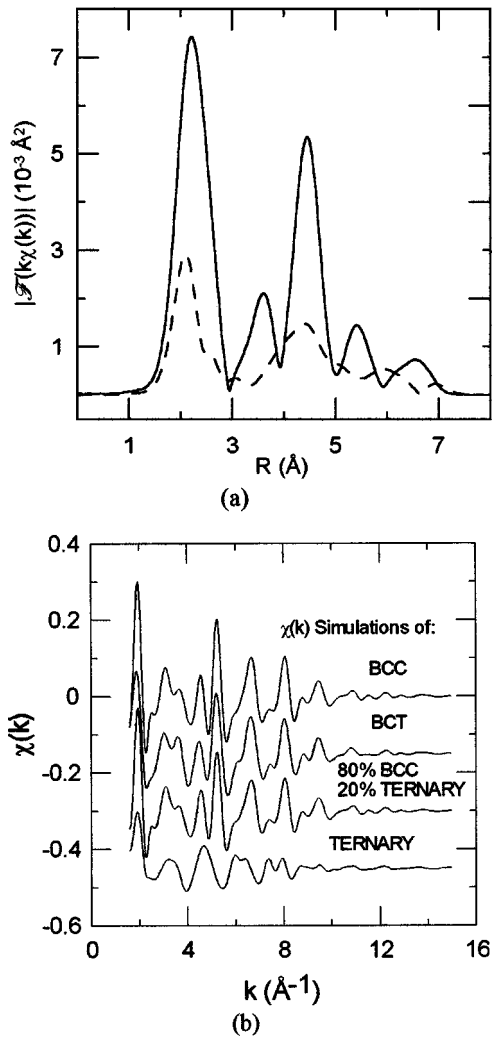

FIG. 6. FEFF7 simulations: (a) *R*-space transforms for bulk iron (solid line) and $Fe_{3.22}Ga_{1.83}As_{0.32}$ ternary compound (dashed line) at 300 K and a Debye temperature of 470 K, and (b) *k*-space EXAFS simulations of bcc Fe, bct Fe, an 80%bcc/20% ternary alloy, and the ternary compound.

from the three iron sites. The results of the simulations, transformed as per the real data, are compared in Fig. 6(a). The most significant difference, apart from scale, lies in the region between 3 and 4 Å. Where the compound has a minimum, bcc iron has a peak containing two triangular multiple-scattering paths (from absorber to nearest neighbor to second-nearest neighbor and back to target absorber, from absorber to nearest neighbor to nearest neighbor in adjoining cell, and back to target absorber) and dominated by backscattering from the face-diagonal position (Fig. 5). Since the data for all three film samples examined here, in both polarizations, possess a similar feature between 3 and 4 Å, we conclude that the films are dominated by a bcc-like structure. We cannot, however, rule out some mixture of phases. In examining the EXAFS simulations of bcc Fe, bct Fe, the ternary compound, and mixtures of bcc and compound, we found the 80% bcc, 20% compound mixture to bear the closest resemblance to bct Fe [Fig. 6(b)]. This suggests 20% alloying would be the sensitivity limit of EXAFS since any higher percentage resulted in suppression of the feature at 5.3 $Å^{-1}$—a feature that is strong in the data in Figs. 2–4.

Auger results[14,15] for films on (4×6)-GaAs have indicated the presence of some ($\lesssim$1 ML[15]) arsenic in the film or floating on its surface after iron deposition. FEFF7 simulations of a 10% random inclusion of arsenic in iron indicate some changes at low *k* due to differences in backscattering. The effects on the nearest and second-nearest neighbor (R_1 and R_2 in Fig. 5) contributions were small, but for higher shells, and particularly for the multiple scattering, the effects were noticeable. In that light, it is possible the differences in the polarization-dependent XANES may be also due to the presence of the substrate (and Au or floating-As capping layers).

The data were fit in *R* space with FEFF7 simulations using the program WINXAS.[30] WINXAS uses the generated Feffnnnn.dat files for each selected scattering path of a particular structural model and generates a $\chi(k)$ using the XAFS function (neglecting cumulants):

$$\chi_{\text{model}}(k)=\sum \frac{S_0^2 N_j F_j(k)}{kR_j^2} e^{(-2k^2o_j^2)} \times e^{[-(2R_j/\lambda)]} \sin[2kR_j+\delta_j(k)]. \quad (2)$$

The resulting $\chi_{\text{model}}(k)$ is transformed to *R* space and compared to the transform of the data.

Fits in *R* space were done over the range 1.6 to 4.1 Å with the aim of extracting the distances for the first three shells—nearest neighbor, lattice parameter, and face-diagonal positions. The main objective of fitting is to obtain the in-plane and out-of-plane lattice parameters. The iron foil data is again used as a reference to determine offsets in *R* and to set the FEFF E_0 shift for the film data. Coordination numbers N_j were fixed according to the models used. While correlations exist between the S_0^2, N_j, and Debye-Waller terms $[\exp(-\alpha_j^2k^2)]$, no significant correlation exists between these terms and the R_j values. For the foil, no polarization dependence was used in FEFF7 and bulk values for N_j were used ($N_1=8$, $N_2=6$, $N_3=12$). For the films, polarization dependence was used.

Polarization dependence in XAFS reduces the degeneracy of some scattering paths (as does the reduction in symmetry from bcc to bct) in a crystalline material. This occurs because of a cosine-squared dependence of the XAFS interference function $\chi(k)$ on the angle, α_j, between the interatomic bond direction R_j and the x-ray polarization vector and causes atoms perpendicular to the polarization vector to contribute little to the backscattering.[31] For polarization along the *c* axis in bcc iron, for example, the six atoms in the second shell (N_2) are no longer equivalent backscatterers. Instead, the two atoms at $(0,0,+/-a)$ dominate. For the rest of this paper, we only enumerate the dominant backscattering atoms in the shells being fit. These values ($N_{j\text{dom}}j=1,2,3$) are reduced from the unpolarized values (8,6,12) of bcc iron to (8,2,8) for polarization along (001) or (010) directions and to (4,4,10) for polarization along (110).

Although the terrace sizes are large,[15] being greater than $60\times100\ Å^2$, the average coordination numbers may be further reduced due to finite thickness.[32] In considering an isolated infinite bcc crystalline sheet and polarization along (001), for example, the numbers are reduced to $N_{1\text{dom}}=7.2$, $N_{2\text{dom}}=1.6$, and $N_{3\text{dom}}=6.4$ for 10 *isolated* monolayers. Scattering from substrate and capping layers, however, will

TABLE II. Summary of fit results for the first three backscattering paths: nearest neighbor, lattice parameter, and face diagonal. An offset correction based on the difference between the foil and bcc crystal R values has been applied to the film fit results. Errors reported were obtained from a doubling of the residual sum of squares from the minimum value. For the third shell of the bct structure, $N_{3\mathrm{dom}}$ has been split into in-plane and out-of-plane values.

Sample	$N_{1\mathrm{dom}}$	R_1 (Å)	σ_1^2 (10^{-4} Å^2)	$N_{2\mathrm{dom}}$	R_2 (Å)	σ_2^2 (10^{-4} Å^2)	$N_{3\mathrm{dom}}$	R_3 (Å)	σ_3^2 (10^{-4} Å^2)	ΔE_0 (eV)	Residual[a] %
bcc Fe crystal	8	2.4824		6	2.8664		12	4.0537			
Fe foil	8	2.462(4)	46(3)	6	2.839(8)	52(6)	12	4.035(17)	95(20)	2.64(50)	2.8
Offset		0.020(4)			0.027(8)			0.019(17)			
bct Fe model crystal											
In-plane (110)	4	2.4828		4	2.8400		2	4.0164			
Out-of-plane (001)	8	2.4828		2	2.9200		8	4.0733			
20Au/10Fe											
In-plane (110)	4	2.495(8)	52(3)	4	2.834(14)	54(4)	2	4.02(5)	79(20)	2.64	3.1
Out-of-plane (001)	8	2.495(9)	47(20)	2	2.93(3)	119(50)	8	4.09(5)	143(50)	2.64	2.4
9.3Fe											
In-plane (010)	8	2.493(9)	40(3)	2	2.837(20)	79(20)	4	4.02(6)	95(40)	2.64	2.6
Out-of-plane (001)	8	2.497(10)	53(26)	2	2.91(5)	142(82)	8	4.08(6)	166(73)	2.64	3.1
20Au/5Fe (S)											
In-plane (110)	4	2.490(10)	45(3)	4	2.862(20)	70(10)	10	4.08(5)	91(30)	2.64	2.8
Out-of-plane (001)	8	2.494(10)	52(10)	2	2.858(23)	75(20)	8	4.05(5)	118(30)	2.64	3.6

[a] $\mathrm{Residual}(\%) = \dfrac{\Sigma |y_{\mathrm{exp}}(i) - y_{\mathrm{calc}}(i)|}{\Sigma |y_{\mathrm{exp}}(i)|} \times 100.$

contribute with different atom type having more effect on the higher shells and on the multiple scattering than on the R_1 and R_2 shells. This will effectively increase the coordination numbers towards bulk (with polarization) crystalline values. We therefore consider a capped infinite sheet model with parameters S_0^2 (scale factor), $\{R_j\}$ (distances), and $\{\sigma_j^2\}$ (mean-square relative displacement) to be fit and N_j's fixed to the bulk, polarization-dependent values.

Table II contains the results of the fits to each sample and orientation. Shells from one orientation required for multiple scattering and face-diagonal paths in the other were fixed to the appropriate fit values and the fitting iterated until stable. The triangular multiple-scattering paths on the low-R side of the R_3 peak were constrained in WINXAS using the parameters for the first and second shells. For the foil, it is evident in Fig. 7(a) that the multiple-scattering region is not being fit perfectly. The fit is worse in this region for the thin-film samples, with the worst case (largest residual) shown for the 5 ML sample (polarization out-of-plane) in Fig. 7(b), presumably due to non-iron atoms contributing to the (multiple) scattering.

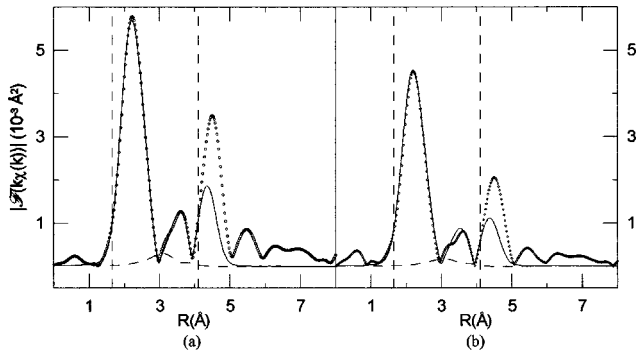

FIG. 7. Comparison of the magnitudes of the Fourier transforms (symbol) and fit (solid line) for (a) iron foil and (b) 20Au/5Fe/GaAs (S) out-of-plane measurements. Vertical-dashed lines indicate the fitting region in R space. The dominant multiple-scattering contribution is also shown (dashed curve).

The fitted foil R values listed in Table II differ from the crystallographic values due to a small systematic offset from usingy FEFF7. An offset correction equal to the difference between the foil fit and crystal R values was applied to obtain the film R values listed in the table. The resulting R_2 values for the 5 ML sample on sulfur-passivated GaAs, indicate a nearly cubic material with a c/a ratio of 1.00(1). The in-plane and out-of-plane R_2 values for the films on (4×6)-GaAs are different, as expected from the beating analysis, with an in-plane contraction and out-of-plane expansion. Some small additional offset due to Ga and As backscattering contributions must also be present. The contraction to 2.834 Å in-plane in the 10 ML film gives a closer match to the underlying GaAs ($a/2 = 2.827$ Å) than assumed in the starting model (2.84 Å). The out-of-plane expansion is slightly different between *in* and *ex situ* samples, but within error. The c/a ratio (Table III) from the 10 ML *ex situ* measurements is 1.03(1) and the ratio from the *in situ* sample is 1.03(2). Both are in agreement and consistent with the value obtained from beating analysis.

An in-plane contraction can be understood as an effort to lattice match to the underlying GaAs ($a/2 = 2.827$ Å) and the expansion an effort to conserve cell volume (Table III) or nearest-neighbor distance (Table II). According to elasticity theory,[33,34] the ratio of the out-of-plane to in-plane strain is $\Delta c/\Delta a = -2c_{12}/c_{11}$. Using the known elastic constants c_{ij},[35] the ratio should be -1.212. The experimental strains for the films, defined by subtracting the lattice parameter of the bcc Fe foil, are tabulated in Table III. Although the errors

TABLE III. Comparison of lattice constants and uniaxial strain for epitaxial iron films on GaAs(001) $\times(4\times6)$ and GaAs(001)-S, passivated using results from the FEFF fitting.

Parameter	Fe crystal	20Au/10Fe	9.3Fe	20Au/5Fe (S)
a (Å)	2.8664	2.834(14)	2.837(20)	2.862(20)
c (Å)	2.8664	2.93(3)	2.91(5)	2.858(23)
c/a	1.000	1.034(12)	1.026(19)	1.00(1)
Volume (a^2c, Å^3)	23.55	23.5(3)	23.4(5)	23.4(3)
$\Delta a = a - a_{\text{crystal}}$ (Å)	0.000	$-0.032(14)$	$-0.029(20)$	$-0.004(20)$
$\Delta c = c - c_{\text{crystal}}$ (Å)	0.000	0.064(30)	0.044(50)	$-0.008(23)$
$\Delta c/\Delta a = -2c_{12}/c_{11}$	-1.212	-2.0 ± 1.3	-1.5 ± 2.0	(ill-defined)

associated with the small differences are large, for the *ex situ* 10 ML film, $\Delta c/\Delta a = -2.0\pm1.3$ is noticeably offset from the bulk-iron value of -1.212. However, for the *in situ* 9.3-ML film and the 5-ML film on sulfur-passivated GaAs no disagreement with macroscopic elasticity theory can be claimed.

How does knowledge of a structural anisotropy or strain affect the potential application of iron films on GaAs for magnetoelectronics? The existence of this strain will affect the interpretation of the uniaxial surface anisotropy. The tetragonal distortion of nickel films on copper, for example, has been shown to dramatically affect the magnetic anisotropy energy.[36] The uniaxial surface anisotropy is typically measured by ferromagnetic resonance and magnetometry. In the saturated state, the effective demagnetizing field perpendicular to the film surface depends on the strain as

$$4\pi M_{\text{eff}} = 4\pi D M_s - \frac{2K_u^s}{M_s d} - \frac{2B_1(e_\perp - e_\parallel)}{M_s}, \qquad (3)$$

where M_s is the bulk magnetization, D is the demagnetizing factor, d is the film thickness, B_1 is the magnetoelastic coupling coefficient (-3.44×10^7 erg/cm^3 for Fe), $e_\parallel$, and $e_\perp$ are the strains parallel and perpendicular to the substrate, and K_u^s is the perpendicular surface anisotropy. Measurements of K_u^s have yielded a value of 1.1 erg/cm^2 (Ref. 15) but this value may have to be modified by a 22% increase if the strain relaxes as $1/d$. Further detailed study of the thickness dependence of the lattice strain is in progress.

IV. CONCLUSIONS

We have used polarized-XAFS studies to examine the structures of two iron films deposited on GaAs(001)-(4×6) surfaces and one on sulfur-passivated GaAs(001), and compared them to the body-centered-cubic structure of an iron foil. The 5 ML sample on sulfur-passivated GaAs exhibits a nearly cubic structure with $c/a = 1.00(1)$. The structures of the 10 ML (*ex situ*) and 9.3 ML (*in situ*) samples on (4×6)-GaAs can be modeled by a tetragonal distortion away from bcc with an in-plane contraction that improves (lessens) the lattice mismatch with GaAs and an out-of-plane expansion that nearly conserves cell volume to give a c/a ratio of 1.03(1).

ACKNOWLEDGMENTS

The Natural Sciences and Engineering Research Council of Canada provided support through operating grants and a major facility access grant. Experiments at the PNC-CAT beamline, Advanced Photon Source, Argonne National Laboratory are also supported by the United States Department of Energy, Basic Energy Sciences, Office of Science under Contract Nos. W-31-109-Eng-38 (APS) and DE-FG03-97ER45628 (PNC-CAT). The authors would also like to thank S. Watkins for the sulfur-passivated substrate.

*Corresponding author.

[1] S. A. Chambers, F. Xu, H. W. Chen, I. M. Vitomirov, S. B. Anderson, and J. H. Weaver, Phys. Rev. B **34**, 6605 (1986).
[2] G. A. Prinz, *Ultrathin Magnetic Structures*, edited by B. Heinrich and J. A. C. Bland (Springer-Verlag, New York, 1994), Vol. 2, Chap. 1.
[3] A. Filipe and A. Schuhl, J. Appl. Phys. **81**, 4359 (1997).
[4] J. J. Krebs, B. T. Jonker, and G. A. Prinz, J. Appl. Phys. **61**, 2596 (1987).
[5] E. M. Kneedler, B. T. Jonker, P. M. Thibado, R. J. Wagner, B. V. Shanabrook, and L. J. Whitman, Phys. Rev. B **56**, 8163 (1997).
[6] M. Gester, C. Daboo, R. J. Hicken, S. J. Gray, A. Ercole, and J. A. C. Bland, J. Appl. Phys. **80**, 347 (1996).
[7] J. L. Simonds, Phys. Today **48**, 26 (1995).
[8] G. A. Prinz, Phys. Today **48**, 58 (1995).
[9] A. Filipe, A. Schuhl, and P. Galtier, Appl. Phys. Lett. **70**, 129 (1997).
[10] B. Lépine, S. Ababou, A. Guivarc'h, G. Jézéquel, S. Députier, R. Guérin, A. Filipe, A. Schuhl, F. Abel, C. Cohen, A. Rocher, and J. Crestou, J. Appl. Phys. **83**, 3077 (1998).
[11] M. Sugiyama, S. Maeyama, and M. Oshima, Phys. Rev. B **50**, 4905 (1994).
[12] G. W. Anderson, M. C. Hanf, X. R. Qin, P. R. Norton, K. Myrtle, and B. Heinrich, Surf. Sci. **346**, 145 (1996).
[13] M. Zölfl, M. Brockmann, M. Köhler, S. Kreuzer, T. Schweinböck, S. Miethaner, F. Bensch, and G. Bayreuther, J. Magn. Magn. Mater. **175**, 16 (1997).
[14] Y. B. Xu, E. T. M. Kernohan, D. J. Freeland, A. Ercole, M. Tselepi, and J. A. C. Bland, Phys. Rev. B **58**, 890 (1998).
[15] T. L. Monchesky, B. Heinrich, R. Urban, and K. Myrtle, Phys. Rev. B **60**, 10 242 (1999).
[16] J. Stohr, in *X-Ray Absorption Spectroscopy: Principles, Applications, Techniques of EXAFS, SEXAFS and XANES*, edited by D. C. Koningsberger and R. Prins (Wiley, New York, 1988), Chap. 10.
[17] E. D. Crozier, Nucl. Instrum. Methods Phys. Res. B **133**, 134

(1997).
[18] K. M. Kemner, B. A. Bunker, A. J. Kropf, H. Luo, N. Samarth, J. K. Furdyna, M. R. Weidmann, and K. E. Neumann, Phys. Rev. B **50**, 14 327 (1994); A. J. Kropf, B. A. Bunker, and J. K. Furdyna, J. Synchrotron Radiat. **6**, 370 (1999).
[19] P. L. Le Fevre, H. Magnan, O. Heckmann, V. Brios, and D. Chandesris, Phys. Rev. B **52**, 11 462 (1995).
[20] H. Oyanagi, K. Sakamoto, R. Shidoa, Y. Kuwahara, and K. Haga, Phys. Rev. B **52**, 5824 (1995).
[21] D. T. Jiang and E. D. Crozier, Can. J. Phys. **76**, 621 (1998).
[22] D. T. Jiang, R. A. Gordon, E. D. Crozier, T. L. Monchesky, and B. Heinrich (unpublished).
[23] S. M. Heald, D. L. Brewe, E. A. Stern, K. H. Kim, F. C. Brown, D. T. Jiang, E. D. Crozier, and R. A. Gordon, J. Synchrotron Radiat. **6**, 347 (1999).
[24] R. A. Gordon, E. D. Crozier, D. T. Jiang, J. Shoults, and E. Hefter (unpublished).
[25] E. D. Crozier and A. J. Seary, Can. J. Phys. **59**, 876 (1981).
[26] G. Martens, P. Rabe, N. Schwentner, and A. Werner, Phys. Rev. Lett. **39**, 1411 (1977).
[27] E. D. Crozier, Physica B **158**, 14 (1989).
[28] S. I. Zabinsky, J. J. Rehr, A. Ankudinov, R. C. Albers, and M. J. Eller, Phys. Rev. B **52**, 2995 (1995).
[29] O. Moze, C. Greaves, F. Bouree-Vigneron, B. Cockayne, W. R. MacEwan, N. A. Smith, and I. R. Harris, J. Phys.: Condens. Matter **6**, 10 435 (1994).
[30] T. Ressler, J. Phys. IV **7**, C2-269 (1997).
[31] The FEFF7 computer code uses the Rehr–Albers formalism to include in the XAFS interference function $\chi(k)$ the contribution of the polarization dependence for each scattering path (Ref. 28) and the equation for $\chi(k)$ does not include the $\cos^2 \alpha_j$ factor explicitly. This differs from earlier treatments (see, for example, Sec. 10.4.1 of Ref. 16) in which the equation for $\chi(k)$ for a K edge contains a multiplicative factor of $3 \cos^2 \alpha_j$ where α_j is the angle between a particular bond R_j and the electric vector of the incident x ray.
[32] E. D. Crozier, A. J. Seary, M. K. McManus, and D. T. Jiang, J. Phys. IV **7**, C2-251 (1997).
[33] W. A. Brantley, J. Appl. Phys. **44**, 534 (1973); J. Hornstra and W. J. Bartels, J. Cryst. Growth **44**, 513 (1978).
[34] B. Heinrich, M. Kowalewski, and J. F. Cochran, Can. J. Chem. **76**, 1595 (1998).
[35] S. Chikazumi and S. H. Charap, *Physics of Magnetism* (Wiley, New York, 1964), p. 173; F. W. Lee, Rep. Prog. Phys. **18**, 184 (1955).
[36] O. Hjortstam, K. Baberschke, J. M. Wills, B. Johansson, and O. Eriksson, Phys. Rev. B **55**, 15 026 (1997).